Control Engineering Practice 168 (2026) 106735

Contents lists available at ScienceDirect

Control Engineering Practice

journal homepage: www.elsevier.com/locate/conengprac

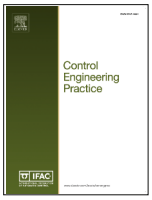

Active control of vehicle lateral dynamics through roll stiffness distribution: Simulation and driver-in-the-loop testing

Samuel Sonnino [a,*], Stefano Melzi [a], Francesco Pirchio [a], Pietro Caresia [b], Alessandro Manzoni [b], Gianluca Vaini [b]

[a] Department of Mechanical Engineering, Politecnico di Milano, Via Giuseppe La Masa 1, Milan, 20156, Italy
[b] R&D, Brembo N.V., Via Stezzano 87, Bergamo (BG), 24126, Italy

ARTICLE INFO

Keywords:
Active suspension
Lateral dynamics
Vehicle stability
Roll stiffness distribution
Active anti-roll bar
Driver-in-the-loop

ABSTRACT

This study investigates the potential of Active Suspension systems to modulate Roll Stiffness Distribution (RSD) with the goal of enhancing vehicle lateral performance and stability. By shifting the suspension's role beyond conventional vertical dynamics and ride comfort, widely explored in existing literature, the proposed approach leverages Roll Stiffness Distribution between front and rear axles to actively influence handling balance across a broad range of driving conditions.

The approach utilizes actuators already integrated into the suspension systems of modern vehicles, maximizing their potential through a dedicated control strategy. A control logic for the active management of RSD is introduced, designed to mitigate understeer or oversteer behavior in real time.

System validation is initially performed in a simulation environment using standardized open-loop maneuvers in accordance with ISO protocols (Ramp Steer, Step Steer, Sine with Dwell). The controller is optimized using a Genetic Algorithm (GA) and subsequently validated through Driver-in-the-Loop (DiL) testing, conducted with a sample of 24 drivers at the dynamic simulator DriSMi of Politecnico di Milano. These tests aimed to assess both objective performance and subjective driver perception.

Finally, the proposed system was integrated into a vehicle equipped with an Active Rear Steering system to explore the synergies between the two control systems and define their respective domains of effectiveness in lateral dynamics optimization.

1. Introduction

Vehicle lateral dynamics and stability are fundamental aspects for both safety and driving performance. Lateral instability is a major contributor to vehicle accidents, especially under high-speed cornering or sudden maneuvers. Among suspension parameters, the distribution of roll stiffness between front and rear axles critically influences understeer/oversteer balance, cornering behavior, and overall driver safety [Dixon, 1996, Jazar, 2008, Mastinu & Plöchl, 2014, Milliken & Milliken, 1995, Pacejka, 2005]. Traditional passive elements, such as springs and anti-roll bars, provide fixed roll stiffness characteristics that cannot adapt to varying driving conditions. Consequently, their design represents a trade-off between comfort and handling, which may not be optimal under all scenarios. Active management of roll stiffness can overcome these limitations, enabling a continuous balance between ride comfort, handling, and vehicle stability.

Several studies have investigated methods to optimize suspension design to enhance ride comfort and vehicle stability [Gao, 2022, Konieczny et al., 2020, Li et al., 2016, Qi et al., 2020, Verros et al., 2005, Zhang et al., 2024]. However, most approaches either rely on fixed design parameters, limiting adaptability, or focus on single-objective control strategies that do not simultaneously address roll control, stability and handling trade-offs. Therefore, there is a need for a systematic method to actively manage Roll Stiffness Distribution (RSD) in real time to improve both safety and driving experience.

The Roll Stiffness Distribution (RSD) between front and rear axles, defined as the ratio of front roll stiffness to total vehicle roll stiffness (Eq. (1)), strongly influences lateral stability and handling performance [Mastinu & Plöchl, 2014, Milliken & Milliken, 1995, Pacejka, 2005]. It depends on the suspension spring roll stiffness $k_{\text{susp},i}$ and Anti-Roll Bar (ARB) roll stiffness $k_{\text{arb},i}$, where i denotes the front or rear axle.

$$RSD = \frac{k_{\text{susp},f} + k_{\text{arb},f}}{k_{\text{susp},f} + k_{\text{arb},f} + k_{\text{susp},r} + k_{\text{arb},r}} \tag{1}$$

* Corresponding author.
E-mail address: samuel.sonnino@polimi.it (S. Sonnino).

https://doi.org/10.1016/j.conengprac.2025.106735
Received 4 June 2025; Received in revised form 11 September 2025; Accepted 19 December 2025
Available online 27 December 2025

A proper stiffness distribution affects both understeer and oversteer balance and the vehicle's behavior in steady-state and transient maneuvers [Reuben et al., 2019]. For example, a stiffer rear axle reduces understeer in steady-state cornering but may induce oversteer in transients. In contrast, increased front stiffness enhances stability in dynamic maneuvers but may reduce front grip during tight turns.

To handle varying driving conditions, RSD can be actively controlled [Nguyen, 2021b, Sagewka et al., 2017]. Active suspension systems and control algorithms enable real-time adjustment, allowing a continuous trade-off between stability and performance.

In this work,a systematic approach for the active management of Roll Stiffness Distribution (RSD) is proposed. The main contributions of the study are:

1. Development of a control strategy for the active management of Roll Stiffness Distribution, designed to influence steering behavior and mitigate understeer or oversteer in real time;
2. Optimization of control parameters using a Genetic Algorithm (GA) to maximize system performance across a broad range of driving conditions;
3. Validation of the proposed approach through both offline simulations using standardized maneuvers (Ramp Steer, Step Steer, Sine with Dwell) and Driver-in-the-Loop (DiL) experiments at the DriSMi dynamic driving simulator (Politecnico di Milano) with 24 drivers, assessing both objective performance and subjective driver perception;
4. Exploration of system integration with Active Rear Steering to evaluate synergies and define the respective domains of effectiveness in enhancing lateral dynamics.

By integrating control design, optimization, and experimental validation, this methodology provides insights into how active suspensions can enhance lateral dynamics, improve driving safety, and adaptively balance stability and handling under varying driving conditions.

2. Suspension technologies

Achieving a specific roll stiffness during driving requires actuators capable of adapting stiffness to the vehicle's dynamic needs. Semi-active suspension systems, which adjust damping based on jounce velocity, are effective in transients but lack control authority in steady-state conditions.

Therefore, to optimize lateral behavior across varied driving scenarios, systems that generate active forces, such as fully active suspensions or active anti-roll bars, are essential. Depending on the integration of active or passive elements, suspension architectures can be classified by their control authority over roll dynamics, comfort, and responsiveness [Alexandru & Alexandru, 2011, Tseng & Hrovat, 2015, Yu et al., 2024].

Active components, like actuators or active anti-roll bars, enable real-time adaptation, whereas passive ones rely on fixed mechanical properties. The following classification outlines typical configurations:

1. **Fully active suspension:** Generates independent active forces at each wheel; no need for traditional anti-roll bars.
2. **Semi-active suspension with active anti-roll bar:** Combines semi-active damping with axle-wide roll stiffness control via active bars; no corner-level independence.
3. **Semi-active suspension with passive anti-roll bar:** Semi-active damping with passive roll stiffness; simpler but limited in roll control.
4. **Passive suspension with active anti-roll bar:** Passive damping combined with active roll stiffness adjustment; improves roll behavior without affecting ride height.
5. **Fully passive suspension:** Both damping and roll stiffness are passive; minimal adaptability.

Table 1 compares common suspension architectures, showing that fully active systems offer the highest level of wheel control and ride comfort, although with increased complexity and cost. Semi-active configurations with either active or passive Anti-Roll Bars strike a balance between performance and affordability, while passive setups are simpler and cheaper but lack real-time roll stiffness control.

2.1. Active anti-roll bars on the market

Several manufacturers have adopted Active Anti-Roll Bars (AARB) to dynamically modulate roll stiffness and Roll Stiffness Distribution [Nguyen, 2021a, Zulkarnain et al., 2012]. These systems, using electric or hydraulic actuators, outperform passive bars in precision but remain limited by actuator torque and the inherent coupling between left and right wheels.

While enhancing stability and comfort during cornering, AARB systems lack the lateral independence of fully active suspensions. Table 2 summarizes current AARB technologies, highlighting actuation types, control strategies, and integration levels. It outlines key features, benefits, and limitations of each solution in the context of vehicle dynamics control.

2.2. Active suspensions on the market

Table 3 compares the most advanced active suspension systems currently on the market. These technologies generate real-time control forces independently at each wheel, enabling direct management of roll, pitch, and heave without mechanical anti-roll components. As a result, they deliver superior ride comfort, handling precision, and adaptability across diverse driving conditions.

2.3. Vehicle parameters influence on lateral dynamics

Vehicle lateral performance and stability are influenced by several key parameters, including tire properties, suspension tuning, and vehicle geometry [Mastinu & Plöchl, 2014, Pacejka, 2005]. The main contributors are:

1. **Tire characteristics**: Define the relationship between lateral force and slip angle, shaping the handling curve.
2. **Center of gravity height**: Affects load transfer, influencing lateral grip between inner and outer tires.
3. **Longitudinal mass distribution**: Alters steering response and dynamic stability.
4. **Lateral load transfer**: Load shifts to the outer tire in cornering, reducing total grip due to tire nonlinearity [Mastinu & Plöchl, 2014].
5. **Longitudinal load transfer**: Braking and acceleration shift normal loads, modifying cornering stiffness and inducing combined slip [Pacejka, 2005].

Table 1
Suspension system types.

System	Control	Independence	Comfort	Response Time	Weight	Complexity
Type 1	Yes	Maximum	Very High	Fast	Very High	Very High
Type 2	Partial	Coupled	High	Medium	High	High
Type 3	Partial	Coupled	Moderate	Medium	Medium	Medium
Type 4	Partial	Coupled	Moderate	Medium	Medium	Medium
Type 5	No	Coupled	Low	Mechanical	Low	Low

Table 2
Active roll control systems by brand.

Brand / System	Technology Type	Main Models
Porsche - PDCC [Porsche, 2020]	Electromechanical/Hydraulic	Cayenne, Panamera
BMW - Dynamic Drive [Group, 2019]	Hydraulic	5/7 Series, X5, X6
Audi - Active ARB (eAWS) [Audi, 2023]	Electromechanical	SQ7, SQ8, A8, Q8
Bentley - Bentley Dynamic Ride [Car and Driver , 2016]	Electromechanical	Bentayga
Lamborghini - LDVA [Lamborghini, 2018]	Electromechanical (Integrated)	Urus

Table 3
Comparison of advanced suspension systems.

Brand / System	Technology Type	Variable Height	Active Anti-Roll
Ferrari - TASV [Ferrari, 2018]	Electromechanical	Yes	Yes
Mercedes - e-ABC [Mercedes-Benz, 2018]	Electro-hydraulic (48V)	Yes	Yes
McLaren - Proactive Chassis [Automotive, 2020]	Interconnected Hydraulic	No	Yes
Lexus - LS 600h/500h [International, 2017]	Pneumatic	Yes	Yes (limited)
Bose - Active Suspension [Corporation, 2017]	Electromagnetic (linear)	Yes	Yes

6. **Suspension and ARB stiffness**: Influence lateral load transfer distribution and front/rear axle behavior.
7. **Drive configuration**: Affects how traction forces and slip are distributed, impacting under/oversteer tendency.

2.4. Impact of lateral load transfer and roll stiffness distribution on handling behaviour

Lateral load transfer during cornering alters the front and rear axle characteristics ($F_{y,i}$ vs. α_i), influencing overall handling [Dixon, 1996, Jazar, 2008, Milliken & Milliken, 1995]. As the vehicle turns, centrifugal force causes load to shift from the inner to the outer wheels (Eq. (2)), quantified as ΔF_z, increasing outer tire load and decreasing inner tire load:

$$\begin{cases} F_{z,inn} = F^0_{z,inn} - \Delta F_z \\ F_{z,out} = F^0_{z,out} + \Delta F_z \end{cases} \tag{2}$$

Where $F^0_{z,inn}$ and $F^0_{z,out}$ are the static normal loads, assumed equal, and $F_{z,inn}$, $F_{z,out}$ are the loads under cornering.

Due to the nonlinear dependence of tire lateral force on vertical load, a well-documented phenomenon in vehicle dynamics and extensively investigated in both indoor and outdoor tire tests [Bian et al., 2014, Colombo et al., 2024, Kasprzak et al., 2007, Nam, 2015, Song et al., 2025], the increase in F_y on the more heavily loaded (outer) tire is smaller than the corresponding decrease on the lightly loaded (inner) tire. As a result, when summing the contributions of both wheels to obtain the axle's equivalent lateral force characteristic, the loss on the unloaded tire is not fully compensated by the gain on the loaded one [Mastinu & Plöchl, 2014, Milliken & Milliken, 1995, Pacejka, 2005]. Consequently, the lateral load transfer reduces the total equivalent lateral force of the axle at a given slip angle, thereby diminishing axle effectiveness and modifying the overall vehicle response.

This phenomenon is illustrated in Fig. 1. On the left, the tire lateral force characteristic (black) is compared with the theoretical axle characteristic (green), obtained as twice the single-tire force when neglecting load transfer effects. On the right, the effect of normal load transfer on the inner and outer wheels is shown: the lateral force reduction on the unloaded wheel exceeds the increase on the loaded one, due to tire nonlinearity. As a result, the equivalent axle characteristic, obtained by summing the two tires contribution, lies below the idealized axle curve which neglects load transfer.

The lateral load transfer on each axle is determined by the relative distribution of roll stiffness between the front and rear axles. In particular, the total vehicle lateral load transfer is apportioned between the front and rear axles according to the Roll Stiffness Distribution (RSD), as expressed in Eq. (3), where h_G and t denote the vehicle's center of gravity height and track width, respectively. The RSD therefore plays a fundamental role in shaping the vehicle's lateral dynamics, as it governs how the vehicle's lateral inertial forces during cornering are shared between the two axles, thereby directly affecting handling balance and stability.

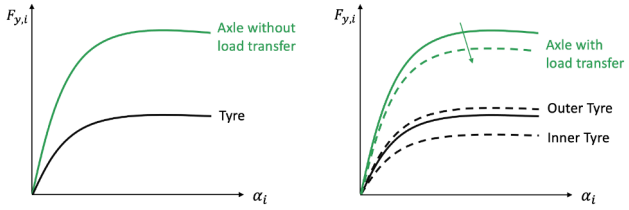

Fig. 1. Effect of lateral load transfer on F_y - α curves.

$$\begin{cases} \Delta F_{z,f} = RSD \cdot \frac{m \cdot a_y \cdot h_G}{t} \\ \Delta F_{z,r} = (1 - RSD) \cdot \frac{m \cdot a_y \cdot h_G}{t} \end{cases} \tag{3}$$

For instance, increasing the front axle roll stiffness (i.e., increasing RSD) shifts a greater portion of load transfer to the front axle, reducing its cornering capability and thus inducing understeer. Conversely, increasing the rear axle roll stiffness (i.e., decreasing RSD) reduces the rear axle's cornering capacity at high lateral accelerations, which may lead to oversteer.

Therefore, by tuning the RSD, either through passive suspension design or by employing active actuators, the handling balance of the vehicle can be modulated in real time, allowing the response to be tailored toward understeer or oversteer as required. Based on this principle, the control strategy proposed in the following section exploits real-time RSD adjustment to achieve the desired lateral vehicle behavior.

3. Control logic

In dynamic conditions, such as high-speed maneuvers or tight cornering, maintaining lateral stability and optimizing handling are critical for safety and performance. To address this, a control logic is designed to adjust the Roll Stiffness Distribution (RSD) in real time, balancing front and rear axle behavior to improve vehicle response.

The control structure includes a feedforward (FF) term that defines a baseline RSD, and a feedback (FB) term that enhances yaw stability by correcting yaw rate deviations. This combination enables adaptation to both understeer and oversteer, ensuring stable and predictable handling.

The approach is actuator-independent: it relies only on vehicle states, allowing implementation with various actuators (e.g., active suspensions or active anti-roll bars) as long as they deliver the commanded forces. In this study, an Active Anti-Roll Bar (AARB) is used.

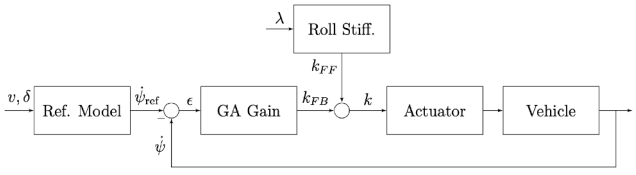

Fig. 2. Block diagram of the control logic.

Fig. 2 shows the control loop, including:

- Yaw rate reference $\dot{\psi}_{ref}$ based on desired handling
- Feedforward stiffness k_{FF} for baseline RSD
- Feedback stiffness k_{FB} from yaw rate error
- Actuator applying the control force
- Vehicle model and actual yaw rate $\dot{\psi}$ closing the loop

3.1. Feedforward contribution

The feedforward term defines a baseline roll stiffness set by the driver via a tuning parameter λ, preserving the original RSD and handling balance while allowing stiffness adjustment. This value remains fixed unless modified by feedback. To increase overall vehicle roll stiffness while preserving the original Roll Stiffness Distribution (RSD), specific increments in stiffness must be applied to the front ($k_{\text{add},f}$) and rear ($k_{\text{add},r}$) Active Anti-Roll Bars (AARB).

The coefficient λ defines the scaling factor of total ARB stiffness in the feedforward configuration. For example:

- $\lambda = 1$: baseline configuration, with $k_{\text{add},i} = 0$
- $\lambda = 1.5$: ARB stiffness increased by 50%

Given a desired λ, tunable by the driver, the added stiffness terms are computed by solving System 4:

$$\begin{cases} RSD = \frac{k_{\text{susp},f}+k_{\text{arb},f}+k_{\text{add},f}}{k_{\text{susp},f}+k_{\text{arb},f}+k_{\text{add},f}+k_{\text{susp},r}+k_{\text{arb},r}+k_{\text{add},r}} \\ k_{\text{arb},f} + k_{\text{add},f} + k_{\text{arb},r} + k_{\text{add},r} = (k_{\text{arb},f} + k_{\text{arb},r}) \cdot \lambda \end{cases} \tag{4}$$

The resulting feedforward stiffness for each axle becomes:

$$k_{FF,i} = k_{\text{arb},i} + k_{\text{add},i} \tag{5}$$

Assuming a linear vertical stiffness, the corresponding actuator force is:

$$F_{FF,i} = k_{lin,FF,i} \cdot \Delta J_i \tag{6}$$

where $k_{lin,FF,i}$ is the linearized feedforward stiffness, and ΔJ_i is the jounce difference between the left and right suspensions on axle i.

3.2. Yaw rate reference

The yaw rate reference sets a target yaw rate consistent with expected vehicle handling. A common expression, based on a single-track model, relates the yaw rate reference $\dot{\psi}_{\text{ref}}$ to steering angle δ and speed v (Eq. (7)):

$$\dot{\psi}_{\text{ref}} = \frac{v}{l(1 + K_{\text{us}} v^2)} \cdot \delta \tag{7}$$

Here, l is the wheelbase and K_{us} the understeering coefficient, dependent on vehicle parameters like mass and tire cornering stiffness.

This linear model holds within the vehicle's linear range. Beyond that, non-linear tire saturation occurs and the reference must adapt. A piecewise function smoothly transitions at a yaw rate threshold $\dot{\psi}^*$ (85% of $\dot{\psi}_{\max}$) corresponding to a steering angle δ^* [Ahangarnejad et al., 2018, 2019, Asperti et al., 2024, De Novellis et al., 2015, Gidlewski & Żardecki, 2017, Gimondi & Corno, 2021, Kissai et al., 2020, Mangia et al., 2021].

The maximum yaw rate $\dot{\psi}_{\max}$ is set by tire-road friction μ (Eq. (8)):

$$\dot{\psi}_{\max} = \frac{\mu g}{v} \tag{8}$$

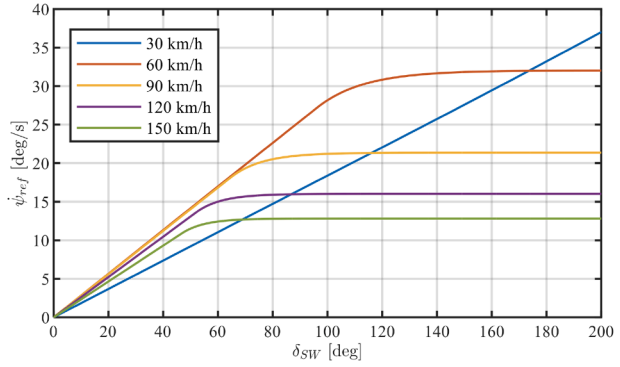

Fig. 3. Reference yaw rate at different running speeds.

The complete yaw rate reference is given by Eq. (9):

$$\dot{\psi}_{\text{ref}} = \begin{cases} \frac{v}{l(1+K_{\text{us}}v^2)}\delta = \alpha\delta & \delta \le \delta^* \\ \dot{\psi}_{\max} + (\dot{\psi}^* - \dot{\psi}_{\max}) e^{\frac{-\alpha(\delta-\delta^*)}{(\dot{\psi}_{\max}-\dot{\psi}^*)}} & \delta > \delta^* \end{cases} \tag{9}$$

Fig. 3 illustrates reference yaw rate vs. steering input at various speeds.

3.3. Feedback contribution

The feedback stabilizes the vehicle by adjusting Roll Stiffness Distribution (RSD) based on yaw rate error ϵ, defined in Eq. (10):

$$\epsilon = |\dot{\psi}_{\text{ref}}| - |\dot{\psi}| \tag{10}$$

Positive ϵ indicates understeer (actual yaw rate lower than reference), negative ϵ indicates oversteer. This sign convention directly links the error to handling conditions.

By monitoring ϵ, the controller adjusts the RSD to improve stability: understeer calls for increased rear axle stiffness and reduced front axle stiffness, oversteer for the opposite.

The feedback stiffness for rear and front axles is (Eq. (11)):

$$\begin{cases} k_{FB,r} = G_j \cdot \epsilon \\ k_{FB,f} = -G_j \cdot \epsilon \end{cases} \tag{11}$$

where G_j is the control gain. For $\epsilon > 0$ (understeer), stiffness is added at the rear and subtracted at the front; for $\epsilon < 0$ (oversteer), the opposite applies.

The total AARB stiffness is the sum of feedforward and feedback components (Eq. (12)):

$$k_i = k_{FF,i} + k_{FB,i} \tag{12}$$

where $k_{FF,i}$ maintains the baseline roll stiffness and RSD according to the parameter λ, and $k_{FB,i}$ adapts to dynamic yaw rate errors.

Actuator force, from the Active Anti-Roll Bar (AARB), is (Eq. (13)):

$$F_{\text{act},i} = (k_{lin,FF,i} + k_{lin,FB,i}) \cdot \Delta J_i \tag{13}$$

with ΔJ_i the suspension jounce difference on axle i, and ($k_{lin,FF,i}$ + $k_{lin,FB,i}$) total linear stiffness applied by the actuator.

Control gains G_j differ for understeer (G_{us}) and oversteer (G_{os}) to tune vehicle-specific handling. The Genetic Algorithm (GA) in Section 4 optimizes these values.

3.4. Actuation

Actuator dynamics is modeled as a first-order filter (Eq. (14)), capturing delay and smoothing control inputs:

$$H(s) = \frac{1}{\tau s + 1} \tag{14}$$

where τ is the filter time constant, representing actuator responsiveness. This simplified model reflects actuator dynamics following [Sagewka et al., 2017] without explicitly modeling motor specifics.

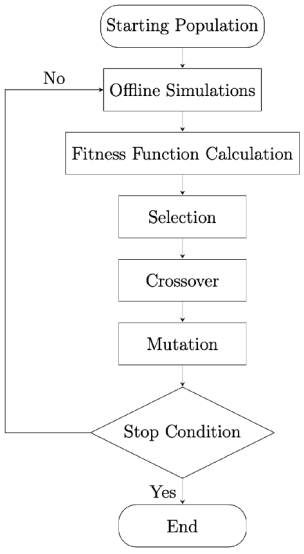

Fig. 4. Flowchart of the GA.

4. Control tuning

A Genetic Algorithm (GA) is used to optimize the control parameters G_{us} and G_{os}, respectively the understeer and oversteer control gains for the developed control logic.

GA is a metaheuristic optimization technique inspired by the principles of natural selection and genetics, where the fittest individuals are selected for reproduction in order to produce the next generation of solutions [Holland, 1975, Katoch et al., 2021].

The algorithm framework, as illustrated in Fig. 4, consists of several key stages: initialization, fitness function calculation, selection, crossover, mutation, and termination.

The objective of the Genetic Algorithm is to maximize vehicle stability and handling performance while minimizing the actuation effort.

The developed GA is divided into different steps:

1. **Initialization of the population:** The GA begins by generating a population of candidate solutions, where each individual is represented by two genes corresponding to the control parameters G_{us} and G_{os}.
   The initial population is generated by selecting these parameters randomly within a constrained range.
   This ensures that the control values are feasible and meet the operational requirements of the actuation system while also promoting genetic diversity and preventing premature convergence of the algorithm.

2. **Fitness function evaluation:** The performance of each individual is evaluated using a fitness function that assesses handling, comfort and actuator effort across three different driving scenarios:
   - Ramp Steer Steady-State test (ISO 4138)
   - Step Steer Transient test (ISO 7401)
   - Sine with Dwell test (ISO 19365)

   Each test is performed at four different speeds ($v = 60, 80, 100, 120$ km/h).
   The offline tests are performed using a 14 Degrees of Freedom (DoF) vehicle model from VI-CarRealTime, integrated with the control model developed within the MATLAB/Simulink environment.
   From the metrics of each test type, certain parameters are selected as Key Performance Indicators (KPIs) to compute the three sub-fitness functions (one for each ISO maneuver considered) that make up the overall fitness function.
   Each sub-fitness function is formulated as a weighted average of three components: handling, comfort, and actuator effort. These components are derived from the KPIs that influence each aspect, allowing for the prioritization of one aspect over the others as needed. At the end, the three sub-fitness functions are combined as a weighted average, given by Eq. (15):

$$\mathrm{FF}(j) = \frac{\sum_i w_i \times ff_i(j)}{\sum_i w_i} \tag{15}$$

   where:
   - $i = SS, T, SD$ defines the test types: steady-state, transient, and sine with dwell
   - j identifies the individual in the population
   - $ff_i(j)$ represents the sub-fitness function of the test i for the individual j
   - w_i denotes the weight assigned to the sub-fitness function i

   and where each sub-fitness function ff_i for the jth individual is expressed as in Eq. (16):

$$ff_i(j) = \frac{\sum_k w_k \times KPIs_{i_k}^{norm}(j)}{\sum_k w_k} \tag{16}$$

   where the weights considered are reported in Table 4, and each $KPIs_{i_k}^{norm}$ represents a KPI for each of the kth aspects considered (comfort, handling, and actuator effort) and is itself composed of a weighted average of other normalized terms upon which each aspect depends. The normalization of each term is performed with respect to the maximum value of that quantity across the individuals within each generation, ensuring comparability among the different quantities. For instance, in the evaluation of comfort, these terms are defined as the peak and steady-state values of accelerations along the three axes, as well as jerk, roll angle, and roll rate. For handling assessment, the considered terms include yaw rate, lateral acceleration, sideslip angle, and settling time. Regarding actuator effort, the terms are represented by the maximum and RMS values of torque and power demand.

3. **Selection:** Individuals with higher fitness scores are more likely to be selected as parents for the next generation. The selection process is stochastic, giving even lower-fitness individuals a chance to be selected to maintain genetic diversity.

4. **Crossover:** The crossover operator combines genetic material from two parent individuals to produce offspring. This mechanism introduces new genetic combinations, aiding the exploration of new solutions.

5. **Mutation:** Mutation introduces random variations in the genes of selected individuals to prevent the population from becoming too homogeneous. The mutation rate is adjusted dynamically based on the diversity of the population, increasing when diversity is low and decreasing when diversity is high. This adaptive strategy enhances the robustness of the optimization process by enabling the GA to escape local optima.

6. **Termination and iteration:** The GA iterates through the aforementioned stages until a termination criterion is met. The algorithm continues until the population converges to a single individual, indicating that no further improvements can be made. The final outcome is the identification of optimal values for G_{us} and G_{os} that balance stability, handling, and actuator effort.

Table 4
Weights for handling, comfort and actuator effort components.

Aspect	Weight	Value
Handling	w_H	1
Comfort	w_C	0.75
Effort	w_E	0.25

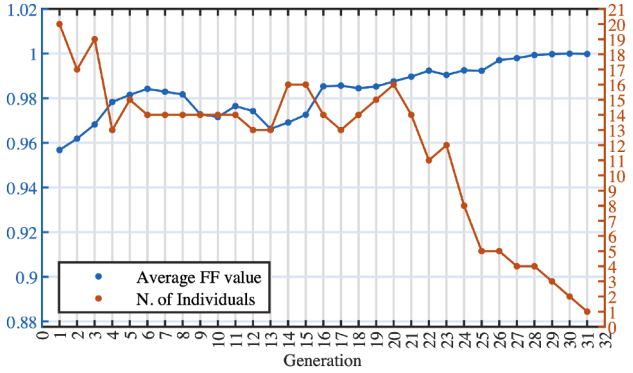

Fig. 5. Evolution of the average FF value and number of distinct individuals throughout the GA run.

Table 5
Threshold values for sideslip angle and actuation.

Parameter	Maximum Value	Unit
Sideslip Angle	6	[deg]
Actuator Force	4500	[N]
Actuator Power	1000	[W]

The algorithm utilized a population of 20 individuals and required 31 generations to reach the stopping criterion.
Fig. 5 depicts the variation in the number of unique individuals throughout the GA run until the best individual eventually dominates and represents the entire population; moreover, the overall fitness function average value progressively increases until convergence is achieved.

The GA imposes penalties on fitness scores for solutions that breach predefined safety constraints. These penalties are applied to ensure that only safe and viable solutions are retained in the optimization process. The safety constraints are:

- Excessive Side Slip Angle: Applied when the side slip angle surpasses a specified safety threshold.
- Actuator Limit Violations: Applied when actuator force or power demands exceed the physical capabilities of the AARB system.

If any of these thresholds are violated, the overall fitness score for that individual is set to zero, effectively discarding the solution from further consideration in the GA.
The threshold values considered are provided in Table 5.

5. Offline testing

The control logic uses the optimized values G_{us} and G_{os} obtained from the Genetic Algorithm, with the feedforward force contribution calculated using $\lambda = 1.5$, representing a 50% increase in initial ARB stiffness compared to the baseline vehicle.
To evaluate the control logic and vehicle dynamics optimization, three maneuvers based on ISO standards (Fig. 6) were selected to ensure repeatability and consistency in performance assessment, covering steady-state and transient conditions.

The first maneuver follows ISO 4138, specifying open-loop tests for steady-state circular driving behavior [International Organization for Standardization, 2021]. The second is based on ISO 7401, which analyzes transient responses to step or sinusoidal steering inputs [International Organization for Standardization, 2011b]. The third uses ISO 19365's sine with dwell test to evaluate stability control effectiveness [International Organization for Standardization, 2016].

These maneuvers form a comprehensive framework for vehicle behavior analysis. Performance is assessed via Key Performance Indicators (KPIs). Tests are performed at four speeds ($v = 60, 80, 100, 120$ km/h), with results at 80 km/h reported here.

Table 6
Vehicle model parameters.

Symbol	Parameter	Value	Unit
m	Vehicle mass	1986.6	kg
I_z	Yaw moment of inertia	3564.7	kg m^2
I_x	Roll moment of inertia	695.7	kg m^2
l	Wheelbase	2.87	m
l_f	CoG to front axle	1.34	m
l_r	CoG to rear axle	1.53	m
h_G	CoG height	0.53	m
t	Track width	1.44	m

Simulations are carried out using a 14 Degrees of Freedom (DoF) vehicle model developed in VI-grade [n.d.] and imported into MATLAB/Simulink, where it is integrated with the control and actuator models. The vehicle is a 4WD fully electric sedan, whose main parameters are reported in Table 6.

VI-CarRealTime is widely adopted in both research and industry to test vehicle control systems, offering a realistic platform for evaluating dynamic behavior prior to experimental validation. The 14 DoF configuration strikes a balance between simplified models (e.g., 2 DoF) and full multi-body simulations, capturing the essential dynamics required for realistic behavior. Vehicle parameters and suspension kinematics, derived from K&C (Kinematics and Compliance) tests on real vehicles, are used to build look-up tables for nonlinear suspension effects (e.g., variations in toe and camber with wheel displacement and steering), ensuring a high-fidelity representation of the vehicle's 3D motion and enabling the creation of a digital twin.

The model describes full-body motion with 6 DoF (three translations and three rotations), while wheel motions relative to the chassis, both translational and rotational, are represented by 8 additional DoF [Cheli et al., 2006, Setiawan et al., 2009]. Tire forces and moments are computed using the Pacejka Magic Formula model [Pacejka, 2005], which reproduces nonlinear tire behavior under combined slip, includes friction dependence on vertical load, and accounts for relaxation effects.

5.1. Ramp steer

The ISO 4138 standard [International Organization for Standardization, 2021] prescribes open-loop tests to assess steady-state circular driving behaviour. The chosen method is a constant speed with a slowly increasing steering-wheel angle (Fig. 6), useful to observe vehicle response as lateral forces rise.

Fig. 7 shows that the Active Anti-Roll Bar (AARB) improves maximum lateral acceleration, especially at medium-high speeds. Table 7 confirms increases in both $a_{y,\mathrm{lin,max}}$ and $a_{y,\mathrm{max}}$. Here, $a_{y,\mathrm{lin,max}}$ is the maximum lateral acceleration within a set error margin based on the linear steering-lateral acceleration relation.

This highlights the system's ability to adapt roll stiffness dynamically, enhancing cornering and reducing understeer. Key observations from Fig. 7 and Table 7 are:

- Yaw rate $\dot{\psi}_{\mathrm{max}}$ and lateral acceleration $a_{y,\mathrm{max}}$ increase with AARB, improving cornering. Though sideslip angle β_{max} rises, it remains within stability limits (Table 5).
- Roll angle ϕ_{max} decreases from 3.1° to 2.6°, thanks to higher initial roll stiffness and effective control logic.

Fig. 8 compares the torque and power required by the two AARBs to achieve the commanded roll stiffness at each axle. These quantities are directly derived from the control objective: the desired AARB stiffness of Eq. (12) and the corresponding force at the wheel hub of Eq. (13). The actuator torque is then computed as the product of this force and the effective lever arm of the AARB mechanism, while the power is determined by multiplying the actuator torque by its angular velocity. In

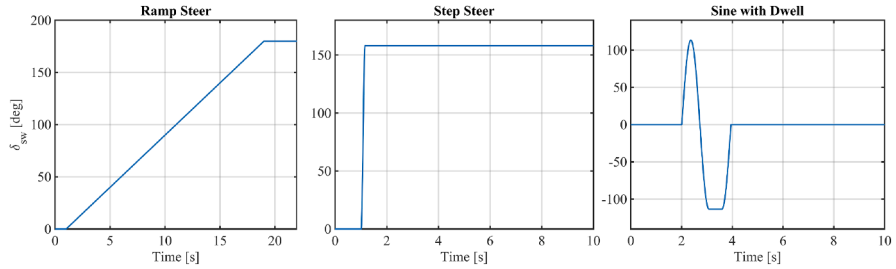

Fig. 6. Steering-wheel inputs for the three maneuvers.

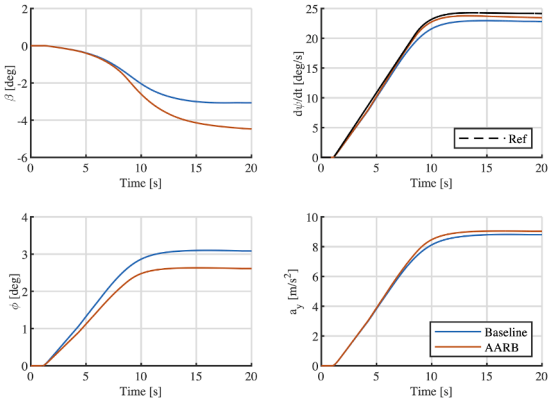

Fig. 7. Sideslip angle, yaw rate, roll and lateral acceleration for ramp steer test.

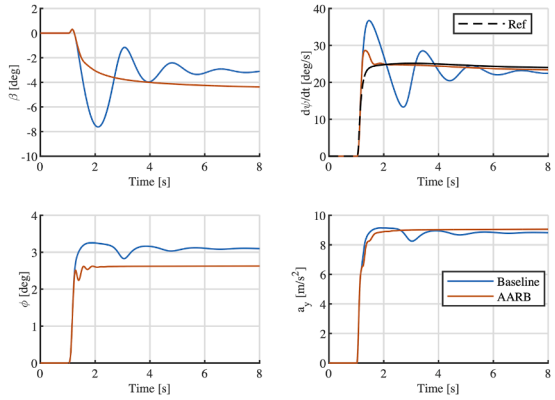

Fig. 9. Sideslip angle, yaw rate, roll and lateral acceleration for step steer test.

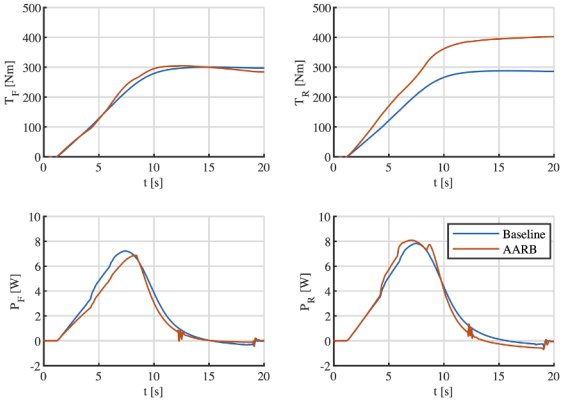

Fig. 8. Torque and power of the two AARB for ramp steer test.

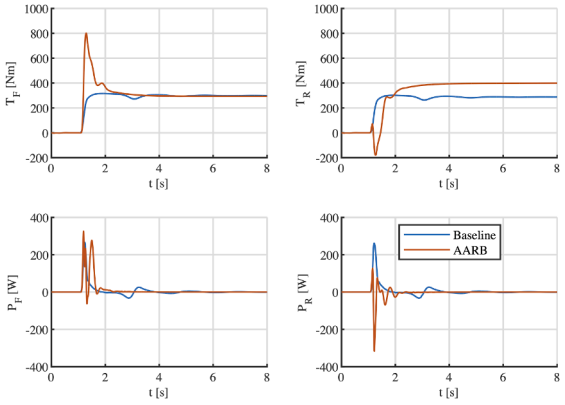

Fig. 10. Torque and power of the two AARB for step steer test.

Table 7
KPIs comparison for ramp steer test.

KPI	Unit	Baseline	AARB	Difference (%)
$a_{y,\text{lin,max}}$	[m/s^2]	7.72	8.30	7.59
$a_{y,\text{max}}$	[m/s^2]	8.82	9.05	2.67
$\dot{\psi}_{\text{max}}$	[deg/s]	22.96	23.77	3.55
β_{max}	[deg]	3.09	4.51	46.09
ϕ_{max}	[deg]	3.10	2.60	−16.13
ϵ_{RMS}	[deg/s]	1.14	0.53	−53.88
ϵ_{max}	[deg/s]	27.16	9.44	−65.23

this way, torque and power plots provide a direct measure of the actuator effort needed to modulate roll stiffness in real time. The results show that the control strategy primarily increases the rear AARB stiffness in order to reduce baseline vehicle understeer tendency.

Overall, the steady-state test confirms that Roll Stiffness Distribution control enhances vehicle handling, predictability, and safety during sustained cornering.

5.2. Step steer

The Step Steer Test applies a rapid steering input at constant speed (Fig. 6), maintained until steady state, to analyze transient vehicle response.

Fig. 9 shows faster stabilization of sideslip, yaw rate, lateral acceleration, and roll angle with AARB, improving safety. Table 8 quantifies settling time reductions: β_{st} down 5.4%, $a_{y,st}$ 41.18%, and $\dot{\psi}_{st}$ 72.64%. AARB also ensures more predictable handling; as the baseline vehicle oscillates between under- and oversteer.

Fig. 10 shows AARB torque and power. Upon oversteer detection, front ARB stiffness rises and rear softens, stabilizing quicker than baseline. Actuator efforts are higher than steady-state test but remain within safe limits (Table 5).

Transient test results confirm that Roll Stiffness Distribution control improves dynamic stability, control precision, and safety during abrupt maneuvers.

Table 8
KPIs comparison for step steer test.

KPI	Unit	Baseline	AARB	Difference (%)
β_{max}	[deg]	7.62	4.43	−41.82
β_{st}	[s]	7.79	7.37	−5.40
β_{ss}	[deg]	−3.10	−4.43	43.11
$a_{y,max}$	[m/s^2]	9.15	9.06	−0.93
$a_{y,st}$	[s]	3.35	1.97	−41.18
$a_{y,ss}$	[m/s^2]	8.82	9.06	2.75
$\dot{\psi}_{max}$	[deg/s]	36.72	28.62	−22.05
$\dot{\psi}_{st}$	[s]	7.20	1.97	−72.64
$\dot{\psi}_{ss}$	[deg/s]	22.67	23.35	3.03
ϵ_{RMS}	[deg/s]	4.14	1.17	−71.82
ϵ_{max}	[deg/s]	12.97	7.40	−42.97
ϕ_{max}	[deg]	3.26	2.63	−19.35
ϕ_{st}	[s]	4.84	1.80	−62.77
ϕ_{ss}	[deg]	3.10	2.63	−15.22
$\dot{\phi}_{max}$	[deg/s]	19.17	18.62	−2.88
$\dot{\phi}_{st}$	[s]	10.00	9.97	−0.25
$\dot{\phi}_{ss}$	[deg/s]	0	0	0
$P_{ARB,\ max}$	[W]	–	325.9	–
$P_{ARB,\ RMS}$	[W]	–	58.6	–
$T_{ARB,\ max}$	[Nm]	–	801.0	–
$T_{ARB,\ RMS}$	[Nm]	–	650.4	–

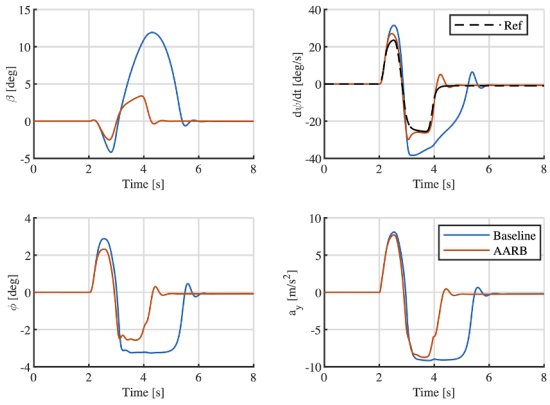

Fig. 11. Sideslip angle, yaw rate, roll and lateral acceleration for sine with dwell test.

Table 9
KPIs comparison for sine with dwell test.

KPI	Unit	Baseline	AARB	Difference (%)
β_{max}	[deg]	8.29	2.35	−71.59
$\dot{\psi}_{max}$	[deg/s]	36.96	28.74	−22.25
$a_{y,max}$	[m/s^2]	9.63	8.43	−12.48
ϕ_{max}	[deg]	3.23	2.63	−18.58
$\dot{\phi}_{max}$	[deg/s]	23.14	18.58	−19.68

5.3. Sine with dwell

The Sine with Dwell Test uses a 0.7 Hz sine steering input with 500 ms dwell (Fig. 6), stressing the vehicle under oscillatory lateral accelerations.

Fig. 11 shows the AARB vehicle's smoother response with reduced sideslip, yaw rate, and lateral acceleration oscillations. Table 9 quantifies reductions in β_{max}, $\dot{\psi}_{max}$, and $\dot{\phi}_{max}$ by 71.59%, 22.25%, and 19.68%, respectively, effectively reducing oversteer and enhancing stability.

Fig. 12 shows torque and power of the AARBs. The control increases front stiffness (and torque) while softening the rear during oversteer.

The test confirms Roll Stiffness Distribution control improves trajectory tracking, reduces body roll, and enhances stability and safety over baseline.

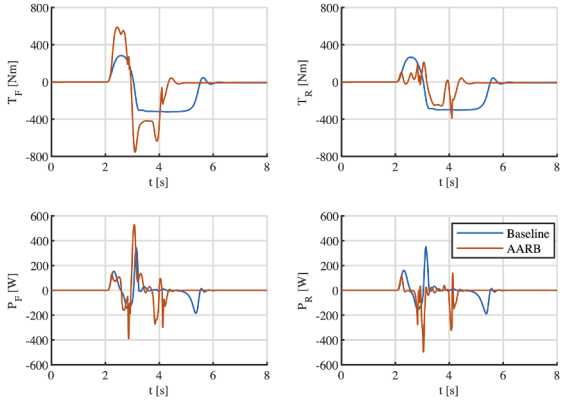

Fig. 12. Torque and power of the two AARB for sine with dwell test.

6. Active rear steer integration

The study focuses on Roll Stiffness Distribution (RSD) control via an Active Anti-Roll Bar (AARB) to improve vehicle stability during demanding maneuvers. Additionally, an Active Rear Steering (ARS) system is implemented in MATLAB/Simulink to investigate potential synergies between the two systems.

The ARS actively adjusts the rear axle steering angle based on vehicle states such as speed, yaw rate, and sideslip angle [Hosseinian Ahangarnejad, 2018], coordinating rear and front wheels to optimize cornering, reduce oversteer/understeer, and enhance handling.

6.1. Linear quadratic regulator

ARS is designed using a Linear Quadratic Regulator (LQR), a popular optimal control method for linear systems [Lewis et al., 2012]. The vehicle's linearized dynamics are:

$$\dot{x} = Ax + Bu. \tag{17}$$

LQR minimizes the cost function

$$J = \int_0^\infty \left(x^T Q x + u^T R u\right) dt \tag{18}$$

where Q and R weigh state error and control effort. The optimal control law is

$$u(t) = -Kx(t) \tag{19}$$

with gain matrix

$$K = R^{-1} B^T P \tag{20}$$

and P solving the Algebraic Riccati Equation

$$A^T P + PA - PBR^{-1} B^T P + Q = 0. \tag{21}$$

6.2. Systems integration

ARS excels in the vehicle's linear operating range, as shown by the Ramp Steer test (Fig. 13), where it improves steering response without increasing maximum lateral acceleration.

In contrast, the AARB-based RSD exploits nonlinear tire and vehicle dynamics at higher lateral accelerations, influencing load transfer and handling limits.

Fig. 13 highlights the complementary roles: ARS controls moderate dynamics precisely within the linear range, while AARB activates near limits to enhance handling. This synergy leverages each system's strengths, ensuring balanced, stable vehicle behavior across diverse conditions.

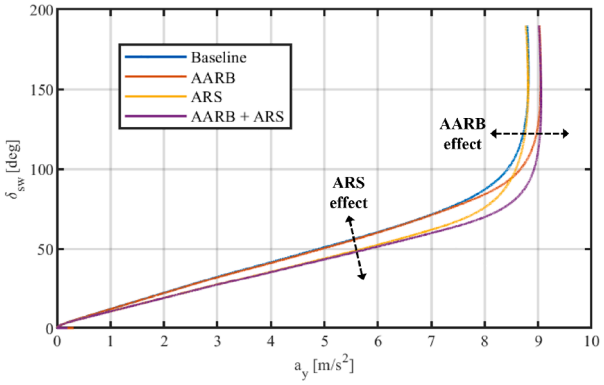

Fig. 13. Ramp steer test with AARB and ARS.

Fig. 14. DriSMi: driving simulator of politecnico di milano.

Fig. 15. Driving scenario (ISO3888-2).

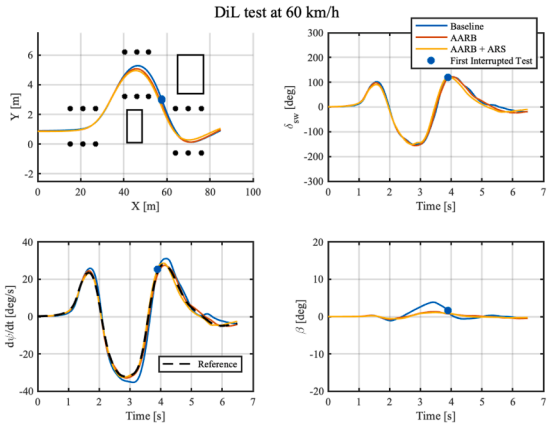

Fig. 16. Test at 60 km/h.

7. Driver-in-the-loop

7.1. Drivers, maneuver and scenario

Driver-in-the-Loop (DiL) testing is performed using the high-fidelity DIM400 driving simulator [VI-grade, n.d.] at Politecnico di Milano DriSMi (Fig. 14). The aim is to assess both objective vehicle performance and subjective driver perception under challenging dynamic conditions.

The DriSMi simulator features a 6x6 m cable-driven platform capable of up to 1.5g accelerations longitudinally and laterally. The cockpit is mounted on a hexalift providing vertical, roll, and pitch motions, surrounded by a 270° curved screen.

The test scenario replicates a double lane change on a three-lane highway (Fig. 15), a standard maneuver to evaluate handling and driver response. The scenario was built in VI-WorldSim, a tool for realistic rendering of driving environments. The layout includes three consecutive cone corridors arranged per ISO3888-2 [International Organization for Standardization, 2011a] standards, with a bus obstacle at the end of each corridor to increase realism and driver immersion. The vehicle reaches target speed before the first cone and coasts through the maneuver by inertia, ensuring driver focus on steering.

Twenty-four participants (12 males, 12 females, aged 19-29) took part, each allowed practice time to familiarize with the simulator. Drivers performed the double lane change at 60, 70, and 80 km/h with different vehicle control setups (Baseline, AARB, AARB + ARS). To reduce learning effects, test sequences were randomized and participants blinded to the control configuration.

Safety limits in the driving simulator restrict side slip angle β to 0.8 rad and its rate to 1 rad/s. Exceeding these thresholds automatically halts the simulation, protecting participants from excessive motions and accelerations.

7.2. Objective results

The data analysis includes trajectories, steering angle (δ_{sw}), yaw rate ($\dot{\psi}$), and side slip angle (β) for all participants. If the side slip angle limits (0.8 rad; 1 rad/s) are exceeded, the simulation halts automatically to ensure safety. The plots mark with a dot the instant the first driver loses control, indicating a change in the number of valid candidates.

Figs. 16–18 show average trajectories and vehicle dynamics (steering angle δ_{sw}, yaw rate $\dot{\psi}$, side slip angle β) for the three configurations (Baseline, AARB, AARB + ARS) at speeds 60, 70, and 80 km/h, respectively, providing a detailed comparison of vehicle behavior during the double lane change.

Trajectories reveal clear differences in lane-switching precision and stability: Baseline shows wider, less consistent paths; AARB is more centralized, indicating better lateral stability; AARB + ARS further narrows and smooths the trajectory, especially in the final cones section.

Steering angle data indicates greater driver effort in Baseline, reduced input with AARB due to active roll stiffness distribution, and minimal corrections with AARB + ARS, showing improved maneuverability.

Yaw rate plots highlight greater fluctuations for Baseline, moderated by AARB, and further stabilized by adding ARS, confirming reduced oscillations.

Side slip angle β is highest in Baseline, indicating lateral instability, reduced with AARB, and lowest with AARB + ARS, confirming enhanced lateral grip and stability.

Differences among configurations grow with speed. At 60 km/h, all metrics differ only slightly, as the maneuver is within the vehicle's limits. At 80 km/h, Baseline shows sharp deviations in yaw and slip angles, while AARB and AARB + ARS maintain better control and stability. The 70 km/h case balances challenge and driver control, showing clear benefits from the active systems without overwhelming natural vehicle response.

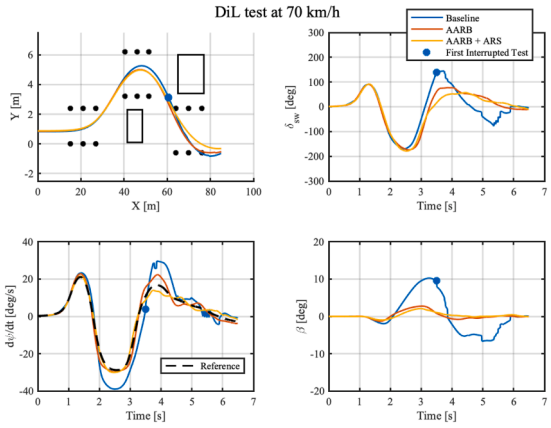

Fig. 17. Test at 70 km/h.

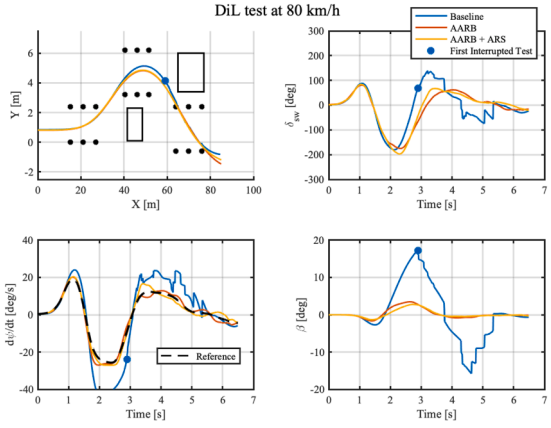

Fig. 18. Test at 80 km/h.

Table 10
Driver configuration preferences.

Speed	Config. Preference	n. of Drivers	Config. Preference	n. of Drivers
60 km/h	Baseline	8	AARB	12
	AARB	16	AARB + ARS	12
70 km/h	Baseline	6	AARB	12
	AARB	18	AARB + ARS	12
80 km/h	Baseline	5	AARB	15
	AARB	19	AARB + ARS	9

Active roll stiffness distribution proves effective in stabilizing during curve peaks with high lateral acceleration, while active rear steering enhances maneuverability during corner exit phases. Their combined effect, as seen in Fig. 13, provides a comprehensive improvement throughout the maneuver.

Overall, control system benefits increase with speed, proving effective in dynamic scenarios where active strategies improve safety and handling.

7.3. Subjective results

After completing maneuvers with randomized vehicle configurations, drivers indicated which vehicle they perceived as more stable and safer. Preferences between Baseline vs. AARB and between AARB vs. AARB + ARS at all the three speeds tested are summarized in Table 10.

Drivers consistently prefer AARB over the Baseline, with preference increasing at higher speeds, confirming objective improvements in stability and highlighting the importance of the proposed control system under more demanding driving conditions. Moreover, when comparing subjective preferences with objective performance data, it becomes evident that the preference for the passive vehicle is not always associated with worse performance under AARB.

This preference discrepancy is likely due to the fact that, in the passive configuration, simulations were terminated when the vehicle approached instability for driver safety reasons, preventing participants from perceiving the full risk of the maneuver and thus leading them to indicate it as their preferred vehicle configuration. To address this limitation, testing with professional drivers, who could safely complete such scenarios without simulation interruption, might be beneficial for future works. In contrast, preferences for the actively controlled vehicle show a stronger alignment between participant ratings and objective performance metrics.

Preferences between AARB and AARB + ARS instead are more balanced, suggesting the ARS benefits are less perceptible during emergency maneuvers under the linear ARS control model. At 80 km/h, more drivers favored AARB alone, indicating that under high dynamic loads the ARS system's advantage is less noticeable subjectively.

8. Conclusions and future developments

In conclusion, the development and evaluation of the Roll Stiffness Distribution (RSD) control via an Active Anti-Roll Bar (AARB) system demonstrated significant improvements in vehicle lateral stability and handling. The research aimed to design and assess an advanced control capable of dynamically adjusting RSD to enhance stability under varied driving conditions, following a structured approach including offline testing, genetic algorithm optimization, and Driver-in-the-Loop (DiL) simulations.

Offline tests quantified notable enhancements: steady-state lateral acceleration increased by 7.59%, transient yaw rate settling time decreased by 72.64%, and sine-with-dwell yaw rate and side slip angle overshoots reduced by 22.25% and 71.59%, respectively.

DiL testing at the DrisMi high-fidelity simulator further validated system performance, with most drivers improving vehicle control and reporting greater confidence during rapid lane changes. Subjective feedback confirmed enhanced stability and responsiveness, especially at higher speeds.

Future research should address robustness under varying conditions, such as:

- Changes in road surface friction requiring adaptive control tuning,
- Variations in tire parameters (e.g., cornering stiffness due to pressure or wear) impacting control accuracy and necessitating compensation.

These aspects are critical to ensure effective performance across diverse scenarios.

Additional avenues for improvement include:

- Integrating roll control alongside yaw rate for comprehensive vehicle dynamics management,
- Incorporating closed-loop maneuvers within genetic algorithm optimization to better mimic real driving,
- Expanding DiL testing to a more diverse driver pool to validate control strategies across different driver profiles.

Overall, the proposed RSD control system shows strong potential to enhance precision and adaptability in vehicle dynamics control, representing a meaningful step toward safer and more responsive handling technologies.

CRediT authorship contribution statement

Samuel Sonnino: Writing – review & editing, Writing – original draft, Visualization, Validation, Supervision, Software, Resources,

Methodology, Investigation, Formal analysis, Data curation, Conceptualization; **Stefano Melzi:** Supervision, Software, Project administration, Formal analysis, Conceptualization; **Francesco Pirchio:** Writing – original draft, Methodology, Data curation; **Pietro Caresia:** Supervision, Methodology, Conceptualization; **Alessandro Manzoni:** Supervision, Methodology, Conceptualization; **Gianluca Vaini:** Supervision, Methodology, Conceptualization.

Declaration of competing interest

The authors declare that they have no known competing financial interests or personal relationships that could have appeared to influence the work reported in this paper.

References

Ahangarnejad, A., Melzi, S., & Ahmadian, M. (2018). Numerical comparison of two methods for integration of active rear steering, torque vectoring and hydraulically interconnected suspension. *International Journal of Vehicle Systems Modelling and Testing*, *13*, 125. https://doi.org/10.1504/IJVSMT.2018.098338

Ahangarnejad, A. H., Melzi, S., & Ahmadian, M. (2019). Integrated vehicle dynamics system through coordinating active aerodynamics control, active rear steering, torque vectoring and hydraulically interconnected suspension. *International Journal of Automotive Technology*, *20*(5), 903–915. https://doi.org/10.1007/s12239-019-0084-x

Alexandru, C., & Alexandru, P. (2011). A comparative analysis between the vehicles' passive and active suspensions. *International Journal of Mechanics*, *5*, 371–378.

Asperti, M., Vignati, M., & Sabbioni, E. (2024). On torque vectoring control: Review and comparison of state-of-the-art approaches. *Machines*, *12*(3), 160. https://doi.org/10.3390/machines12030160

Audi, A. G. (2023). Audi SQ8 - adaptive air suspension plus, eAWS, sport differential and all-wheel steering. https://www.audi-technology-portal.de.

Automotive, M. (2020). Proactive chassis control II. mclaren technology. https://www.mclaren.com.

Bian, M., Chen, L., Luo, Y., & Li, K. (2014). A dynamic model for tire/road friction estimation under combined longitudinal/lateral slip situation. (*vol. 1*). https://doi.org/10.4271/2014-01-0123

Car and Driver (2016). Deep dive: Bentley dynamic ride explained. https://www.caranddriver.com.

Cheli, F., Leo, E., Mancosu, F., & Melzi, S. (2006). A 14 dof model for the evaluation of vehicle's dynamics, numerical-experimental comparison. *Meccanica*, *41*, 35–43.

Colombo, F., Sonnino, S., Mantovani, F., Ronchi, A., Michielan, L., Vignati, M., & Sabbioni, E. (2024). Laboratory abrasion tester to estimate tyre grip and cornering stiffness. In G. Mastinu, F. Braghin, F. Cheli, M. Corno, & S. M. Savaresi (Eds.), *16th international symposium on advanced vehicle control* (pp. 571–577). Cham: Springer Nature Switzerland.

Corporation, B. (2017). Active suspension technology. bose automotive innovations. https://www.bose.com.

De Novellis, L., Lenzo, B., Sabbioni, E., Sorniotti, A., Gruber, P., & Toso, D. (2015). Driving modes for designing the cornering response of fully electric vehicles with multiple motors. *Mechanical Systems and Signal Processing*, . https://doi.org/10.1016/j.ymssp.2015.03.024

Dixon, J. C. (1996). Tires, suspension and handling. (2nd ed.). Warrendale, PA: SAE International.

Ferrari, S. p. A. (2018). Ferrari advanced suspension system: TASV. technical documentation. https://www.ferrari.com.

Gao, J. (2022). Analysis and optimization of suspension spring stiffness for improving frequency response characteristics of the vehicle. *Mathematical Problems in Engineering*, *2022*. https://doi.org/10.1155/2022/9557483

Gidlewski, M., & Żardecki, D. (2017). Linearization of the lateral dynamics reference model for the motion control of vehicles. *Mechanics Research Communications*, *82*, 49–54. https://doi.org/10.1016/j.mechrescom.2016.11.002

Gimondi, A., & Corno, M. (2021). A mixed sideslip yaw rate stability controller for over-actuated vehicles. In *Proceedings of the ASME 2021 international design engineering technical conferences and computers and information in engineering conference (IDETC-CIE)*. https://doi.org/10.1115/DETC2021-68260

Group, B. (2019). BMW 7 series - chassis and suspension. https://www.press.bmwgroup.com.

Holland, J. H. (1975). Adaptation in natural and artificial systems. University of Michigan Press.

Hosseinian Ahangarnejad, A. (2018). Integrated control of active vehicle chassis control systems. Ph.D. thesis. Politecnico di Milano.

International, L. (2017). Lexus LS 500h - chassis and suspension. https://www.lexus.com.

International Organization for Standardization (2011a). ISO 3888-2:2011 - passenger cars – test track for a severe lane-change manoeuvre – Part 2: Obstacle avoidance. Technical Report ISO. https://www.iso.org/standard/57253.HTML.

International Organization for Standardization (2011b). ISO 7401: Road vehicles – lateral transient response test methods – open-loop test methods. Technical Report ISO.

International Organization for Standardization (2016). ISO 19365: Passenger cars – validation of vehicle dynamic simulation – sine with dwell stability control testing. Technical Report ISO.

International Organization for Standardization (2021). ISO 4138: Passenger cars – steady-state circular driving behaviour – open-loop test methods. Technical Report ISO.

Jazar, R. N. (2008). Vehicle dynamics: Theory and application. New York, NY: Springer. https://doi.org/10.1007/978-0-387-74244-1

Kasprzak, E., Lewis, K., & Milliken, D. (2007). Tire asymmetries and pressure variation in the radt/milliken nondimensional tire model. *SAE International Journal of Passenger Cars - Mechanical Systems*, *115*. https://doi.org/10.4271/2006-01-1968

Katoch, S., Chauhan, S. S., & Kumar, V. (2021). A review on genetic algorithm: Past, present, and future. *Multimedia Tools and Applications*, *80*, 8091–8126.

Kissai, M., Monsuez, B., Tapus, A., Mouton, X., & Martinez, D. (2020). Optimal yaw rate control for over-actuated vehicles. In *Wcx sae world congress experience*. Detroit, United States. https://hal.science/hal-02525997.

Konieczny, J., Sibielak, M., & Rączka, W. (2020). Active vehicle suspension with anti-roll system based on advanced sliding mode controller. *Energies*, *13*(21). https://doi.org/10.3390/en13215560

Lamborghini, S. p. A. (2018). Lamborghini Urus - lamborghini dinamica veicolo attiva (LDVA). https://www.lamborghini.com.

Lewis, F. L., Vrabie, D., & Syrmos, V. L. (2012). Optimal control. John Wiley & Sons.

Li, Z.-X., Xu, R.-Z., & Jiang, H. (2016). Roll stiffness optimization for anti-roll bar in interconnected air suspension, . *19*, 293–302. https://doi.org/10.6180/jase.2016.19.3.07

Mangia, A., Lenzo, B., & Sabbioni, E. (2021). An integrated torque-vectoring control framework for electric vehicles featuring multiple handling and energy-efficiency modes selectable by the driver. *Meccanica*, *56*(5), 991–1010. https://doi.org/10.1007/s11012-021-01317-3

Mastinu, G., & Plöchl, M. (2014). Road and off-road vehicle system dynamics handbook. CRC Press.

Mercedes-Benz, A. G. (2018). The new mercedes-benz GLE: The SUV trendsetter completely reconceived. https://media.mercedes-benz.com.

Milliken, W. F., & Milliken, D. L. (1995). Race car vehicle dynamics. Warrendale, PA: Society of Automotive Engineers.

Nam, K. (2015). Application of novel lateral tire force sensors to vehicle parameter estimation of electric vehicles. *Sensors*, *15*, 28385–28401. https://doi.org/10.3390/s151128385

Nguyen, T. A. (2021a). Control the hydraulic stabilizer bar to improve the stability of the vehicle when steering. *Mathematical Modelling of Engineering Problems*, *8*, 199–206. https://doi.org/10.18280/mmep.080205

Nguyen, T. A. (2021b). Improving the stability of the passenger vehicle by using an active stabilizer bar controlled by the fuzzy method. *Complexity*, *2021*, 1–20. https://doi.org/10.1155/2021/6569298

Pacejka, H. (2005). Tire and vehicle dynamics. Elsevier.

Porsche, A. G. (2020). Telaio E sistemi per La dinamica Di guida - I nuovi modelli panamera hybrid. https://newsroom.porsche.com.

Qi, H., Zhang, N., Chen, Y., & Tan, B. (2020). A comprehensive tune of coupled roll and lateral dynamics and parameter sensitivity study for a vehicle fitted with hydraulically interconnected suspension system. *Proceedings of the Institution of Mechanical Engineers, Part D: Journal of Automobile Engineering*, *235*, 095440702094428. https://doi.org/10.1177/0954407020944287

Reuben, E., Budhiraja, R., N, S., K, R. et al. (2019). Evaluating effects of roll stiffness change at front and rear axles on vehicle maneuverability and stability. Technical Report SAE Technical Paper 2019-28-2406. https://doi.org/10.4271/2019-28-2406

Sagewka, S., Fiebig, T., Schmid, C., & Wostal, D. (2017). Mechatronic roll control for the 48-V electrical system. *ATZ Worldwide*, *108*(11), 28–33.

Setiawan, J. D., Safarudin, M., & Singh, A. (2009). Modeling, simulation and validation of 14 DOF full vehicle model. In *International conference on instrumentation, communication, information technology, and biomedical engineering 2009* (pp. 1–6). Bandung, Indonesia. https://doi.org/10.1109/ICICI-BME.2009.5417285

Song, Z., Zhang, S., Li, W., Gan, Y., & Ding, H. (2025). Sensitivity analysis and uncertainty bounding of tire parameters on vehicle handling and stability. *Nonlinear Dynamics*, (pp. 1–34). https://doi.org/10.1007/s11071-025-11446-z

Tseng, H. E., & Hrovat, D. (2015). State of the art survey: Active and semi-active suspension control. *Vehicle System Dynamics*, *53*(7), 1034–1062. https://doi.org/10.1080/00423114.2015.1037313

Verros, G., Natsiavas, S., & Papadimitriou, C. (2005). Design optimization of quarter-car models with passive and semi-active suspensions under random road excitation. *Journal of Vibration and Control*, *11*, 581–606. https://doi.org/10.1177/1077546305052315

VI-grade Dim400 - cable-driven dynamic simulator. https://www.vi-grade.com/en/products/cable-driven_dim_dynamic_simulator/.

VI-grade. Vi-carrealtime - multibody real-time simulation for automotive applications. https://www.vi-grade.com/en/products/vi-carrealtime/.

Yu, M., Evangelou, S. A., & Dini, D. (2024). Advances in active suspension systems for road vehicles. *Engineering*, *33*, 160–177. https://doi.org/10.1016/j.eng.2023.06.014

Zhang, S., Li, M., Li, J., Xu, J., Wang, Z., & Liu, S. (2024). Research on ride comfort control of air suspension based on genetic algorithm optimized fuzzy PID. *Applied Sciences*, *14*, 7787. https://doi.org/10.3390/app14177787

Zulkarnain, N., Imaduddin, F., Zamzuri, H., & Mazlan, S. (2012). Application of an active anti-roll bar system for enhancing vehicle ride and handling. (pp. 260–265). https://doi.org/10.1109/CHUSER.2012.6504321